SMC-TR-94-13

AEROSPACE REPORT NO.
TR-93(3935)-11

Torque Characteristics of Solid Lubricated Precision Bearings During Oscillatory Motion

31 January 1994

Prepared by

R. BAUER and P. D. FLEISCHAUER
Mechanics and Materials Technology Center
Technology Operations

Prepared for

SPACE AND MISSILE SYSTEMS CENTER
AIR FORCE MATERIEL COMMAND
2430 E. El Segundo Boulevard
Los Angeles Air Force Base, CA 90245

Engineering and Technology Group

THE AEROSPACE CORPORATION
El Segundo, California

This report was submitted by The Aerospace Corporation, El Segundo, CA 90245-4691, under Contract No. F04701-93-C-0094 with the Space and Missile Systems Center, 2430 E. El Segundo Blvd., Los Angeles Air Force Base, CA 90245. It was reviewed and approved for The Aerospace Corporation by S. Feuerstein, Principal Director, Mechanics and Materials Technology Center. Col. J. A. Goyette was the project officer for the Mission-Oriented Investigation and Experimentation (MOIE) program.

This report has been reviewed by the Public Affairs Office (PAS) and is releasable to the National Technical Information Service (NTIS). At NTIS, it will be available to the general public, including foreign nationals.

This technical report has been reviewed and is approved for publication. Publication of this report does not constitute Air Force approval of the report's findings or conclusions. It is published only for the exchange and stimulation of ideas.

JOHN A. GOYETTE, Col, USAF
System Program Director
Defense Meteorological Satellite
Program

WILLIAM KYLE SNEDDON, Capt, USAF
Deputy, Industrial & International Division

REPORT DOCUMENTATION PAGE

Form Approved
OMB No. 0704-0188

1. AGENCY USE ONLY (*Leave blank*)	2. REPORT DATE	3. REPORT TYPE AND DATES COVERED
	31 January 1994	

4. TITLE AND SUBTITLE
Torque Charateristics of Solid Lubricated Precision Bearings During Oscillatory Motion

5. FUNDING NUMBERS
F04701-93-C-0094

6. AUTHOR(S)
Bauer, Reinhold; Fleischauer, Paul D.

7. PERFORMING ORGANIZATION NAME(S) AND ADDRESS(ES)
The Aerospace Corporation
Technology Operations
El Segundo, CA 90245-4691

8. PERFORMING ORGANIZATION REPORT NUMBER
TR-93(3935)-11

9. SPONSORING/MONITORING AGENCY NAME(S) AND ADDRESS(ES)
Space and Missile Systems Center
Los Angeles Air Force Base
Los Angeles, CA 90009-2960

10. SPONSORING/MONITORING AGENCY REPORT NUMBER
SMC-TR-94-13

11. SUPPLEMENTARY NOTES

12a. DISTRIBUTION/AVAILABILITY STATEMENT
Approved for public release; distribution unlimited

12b. DISTRIBUTION CODE

13. ABSTRACT (*Maximum 200 words*)

MoS_2 sputter-coated as well as uncoated (bare) angular-contact ball bearings were tested with various cage materials in a low-speed regime. Various self-lubricating polymers either "neat" or with additives and metallic cages were tested. The emphasis of this paper is to report on significant torque increases "torque bumps" observed during non-ball overlap, oscillatory motion for some race/cage combinations. In some race/cage combinations torque bumps can be minimized by proper run-in. No attempt was made to run the bearings to failure, although certain race/cage combinations did in fact fail before the end of test.

14. SUBJECT TERMS
solid lubrication, MoS_2, cage, retainer, composite, self-lubricating

15. NUMBER OF PAGES
37

16. PRICE CODE

17. SECURITY CLASSIFICATION OF REPORT	18. SECURITY CLASSIFICATION OF THIS PAGE	19. SECURITY CLASSIFICATION OF ABSTRACT	20. LIMITATION OF ABSTRACT
UNCLASSIFIED	UNCLASSIFIED	UNCLASSIFIED	

PREFACE

This work was supported under Air Force Materiel Command, Space and Missile Systems Center, contract no. F04701-93-C-0094.

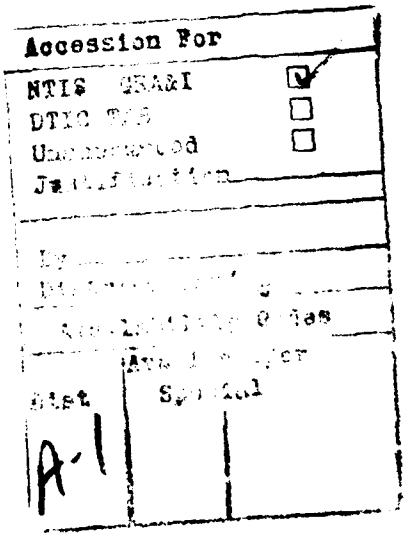

CONTENTS

FIGURES

TABLES

INTRODUCTION

Spacecraft systems containing Moving Mechanical Assemblies (MMAs) at times require solid lubricants (such as MoS_2 and PTFE) rather than fluid lubricants (oils or greases). Factors favoring the use of solid lubricants are (a) low or negligible outgassing properties, (b) low-temperature lubrication (compared to liquids), (c) simplified mechanical design (no need for labyrinth seals, reservoirs, or oilers), and (d) effectiveness under boundary lubrication conditions.[1,2] Recently, tribological assessments and review articles surveying present and future tribological requirements for existing MMA technologies (sliding and rolling contact) have been published.[3-5] More numerous are reports of measurements of the tribological performance, that is, friction or wear life, of solid-lubricated bearings (angular contact or deep groove). Such investigations were conducted by varying physical parameters such as load and speed, or by varying the material composition of the bearing cage or solid lubricant applied to the races.[6-15]

When solid lubricants are used, certain precautions depending on the material are necessary. For example, if MoS_2 is present as the lubricant or a component thereof, storage and testing should be done in dry nitrogen or vacuum, as oxidation of MoS_2 can occur with tribologically detrimental effects.[6,16] Some cage materials (notably the polyimide-based resins) absorb water, necessitating storage in a "dry" environment prior to use.

Another potential problem of solid lubricants that manifests itself during bearing operation is the tendency to form torque "bumps" at or near the end of ball travel when the bearing is operating in a non-ball overlap oscillatory mode. Although this potential pitfall appears to be generally known in industry[17,18] and can be avoided by occasional exercising (rotating) over a large enough angle to ensure ball-ball overlap, scant documentation has been found where this issue has been even partially studied.[19] The objectives of this study were to (a) investigate various commonly employed or potentially new cage materials to determine whether they form torque bumps, (b) measure the rate of bump formation, and (c) determine the physical modifications occurring in the transfer film during testing that contribute to torque-bump formation.

APPARATUS AND TEST SAMPLES

A description of the angular-contact bearing used throughout the tests is given in Table 1. Table 2 lists the cage materials used, with a short description of each.

BEARING TEST FIXTURE (BTF)

The bearing test fixture (BTF) is shown schematically in Fig. 1. All wear testing was performed in vacuum at approximately 5.3×10^{-4} Pa (4×10^{-6} Torr) using a turbomolecular pump backed by a rotary vane pump. A programmable drive/motor system that included a microstep motor (12,800 steps rev^{-1}) and an absolute encoder was mounted outside the vacuum chamber. The shaft (inner-race) position is reported with reference to an arbitrary drive shaft position D0 (HOME); one full rotation would therefore be reported as D12800. This method of position reporting (Dxxxxx) is used throughout this report. A magnetic rotary feedthrough coupled the motor to the BTF's precision shaft inside the chamber where a single-angular contact test bearing is mounted and clamped into place. Load is applied to the BTF housing via a stranded cable that is centered by way of an X-Y positioning stage directly above the center of rotation. A steel rod mounted on the BTF housing transmitted the bearing torque to a high-impedance force transducer capable of measuring both tension and compression. Data were recorded on a computer at 400 Hz for 10 seconds unless otherwise noted.

BEARING AND CAGE COMBINATIONS

Most bearing races were run dry with lubrication provided solely by the self-lubricating (active) cages. A few races, when combined with nonlubricating (benign) cages, were tested with nominally 1-μm-thick, rf-sputtered films containing alternate layers of MoS_2 and Ni. More details on this layered thin-film deposition technique are provided elsewhere.[20] Table 3 lists the 14 race/cage combinations used. Note that duplicate tests were run for each configuration.

TEST PROCEDURE

The following is a description of the typical test procedure. Modifications to the procedure are noted where appropriate. After the bearing is secured in the BTF and the force transducer mounted, the entire system is pumped down to the aforementioned pressure. The bearing was first run-in unidirectionally at low load 90 N (20 lb: 53 ksi, 0.36 GPa) and low speed (30 rpm) for 1,000 revolutions, followed by 9,000 revolutions at the same low load but at 180 rpm. This run-in procedure of 10,000 revolutions (10 KR) under low-stress conditions was used to facilitate transfer of material from the self-lubricating (active) cages onto the balls and races. For the remainder of the test the load was increased to 147 N (33 lb), which resulted in a mean Hertzian stress of 0.5 GPa (73 ksi), with the speed remaining constant at 180 rpm. The bearings were run a total of 1.3 million revolutions unidirectionally, with intermittent pauses at selected cumulative revolutions where small-angle oscillatory movements (i.e., dithers) were to be performed. In most cases the intermittent pauses for dithering took place at the following cumulative revolutions run-in: 20 KR, 78 KR, 108 KR, 308 KR, and 1,300 KR.

STANDARD MOTOR INSTRUCTIONS

Two motor instructions are used in this paper unless otherwise noted. A 300-step dither motion is used to produce the torque bumps, followed by a 600-step survey scan which was used to detect whether torque bumps were in fact created. The survey scan incorporated the original 300-step dither plus an additional 150 steps at both ends of the dither zone (Fig. 2). The following is a detailed description of both motor instructions:

A. Survey Scan (600 steps)

1. Define the HOME position (D0).
2. Move the shaft (inner race) to D600 (16.8°) at an angular velocity of 7.2° sec^{-1}.
3. Leave motor at rest (pause) for 0.5 to 1 second.
4. Return to HOME (D0).
5. Repeat steps 2–4.

B. Dither Zone (300 steps)

6. Position shaft at D150.
7. Oscillate 200 times between D150 and D450 (8.4°) at an angular velocity of 108° sec^{-1}.
8. After dithers, move back to HOME (D0).
9. Repeat the "survey scan" to determine if torque bumps were formed (computer data acquisition: Steps 2–4 above).

10. Repeat steps 6–9 for 600, 1200, 2000, 5000, and 15000 dithers.

11. Rotate bearing unidirectionally to next cumulative run-in pause point (at 20K, 78K, 108K, 308K, and 1300K revolutions).

12. Repeat steps 1–11.

RESULTS

TORQUE AND WEAR LIFE

Torque Bumps

Figure 3 is an example of the torque output during a survey scan prior to dithering. The abscissa represents time and the ordinate the torque. Between Points A and B the motor is positioned at D0 (HOME) and is motionless, as reflected in a near-zero torque output. At Point B the motor begins to move towards D600, causing the torque to increase abruptly for a fraction of a second before settling down to a relatively smooth torque. Once D600 has been reached, the motor halts (Point C) and remains at rest till Point D, where the motor reverses direction and returns back to D0 (Point E). After a short delay the cycle is repeated once more. The D150 and D450 locations are shown to illustrate where the dither scan is to take place.

Two methods (maximum-to-minimum torque and torque-noise) were used where appropriate in reporting the torque of the BTF. The maximum-to-minimum torque value is obtained by taking the difference between the highest and lowest value during the entire survey scan and then dividing by two. The resulting value represents the maximum torque of the system when rotating unidirectionally. In contrast, the torque-noise method is simply a peak-to-peak measurement of the single largest torque bump recorded. The torque-noise method focuses exclusively on the torque bump itself, disregarding the mean torque of the BTF system altogether, and is more useful for gaining insight into the evolution of the torque bumps and factors leading to their development, such as cage material and transfer-film thickness.

Figure 4 is a typical example of the torque-bump buildup as a function of total dithers after 1.3 million revolutions. The uppermost trace is the baseline torque (prior to dithering) and below it are the four results from 200, 600, 2000, and 15000 dithers. For clarity the plots represent single scans that are truncated showing only the first ~4 seconds (one unidirectional motion) rather than the usual 10-second bidirectional survey scan (see Fig. 3). In this particular example, computer-curve-fitting results show the torque of the system (at zero dithers) to be 0.020 N-m (2.89 oz-in.). After only 200 dithers, the maximum-to-minimum torque rose to 0.030 N-m (4.31 oz-in.), an increase of 50%. At 600 dithers, the torque was calculated to be 132% higher than the baseline torque. In most instances the torque bumps increased exponentially until their asymptotic limit had been reached, usually between 1500 to 3000 dithers; thereafter the torque signal increased in a linear fashion. Equation (1) was used to describe the evolution of a torque bump as a function of dithers for both the maximum-to-minimum method and the torque-noise method.*

$$\tau(D) = \alpha(1 - e^{-\beta D}) + (\lambda D) + \rho \qquad (1)$$

* Torque bumps are smoothed out during following run-in phase.

$\tau(D)$ = torque (both methods)

D = number of dithers

α = limiting exponential torque

ρ = mean torque of the system (max - min method only)

$\lambda = f$ (linear bump evolution rate)

$\beta = f$ (exponential bump evolution rate)

A typical example of the increase in the torque bump as a function of the number of dithers for each cumulative run-in is shown in Fig. 5 (torque-noise method; active-cage bearing). Actual data points are shown along with the curve resulting from Eq. (1). The increase in the torque bump as described in Eq. (1) is observed for all the active-cage bearings (P/N 11 through P/N 20), except at 20,000 revolutions, where little if any increases in torque were usually observed. In fact, only three of the ten active-cage bearings tested (P/Ns 11, 13, and 16) showed an increase in their maximum-to-minimum torque to levels that were at least 50% above the predither torque value at 20,000 cumulative run-in revolutions. At 78,000 revolutions and beyond, most active-cage bearings were developing large torque bumps. This trend, where the rate of the maximum-to-minimum torque buildup is directly proportional to cumulative revolutions, can be seen more clearly in Fig. 6, in which the number of dithers required to increase the mean torque of the system prior to dithering (nominally ~0.010 N-m to 0.021 N-m; ~1.5 to 3.0 oz-in.) by 50% is plotted as a function of cumulative revolutions for the various bearings tested. Note again that at 20,000 revolutions only three bearings showed the 50% increase, and they required between 1170 to 4350 dithers to do so (an arbitrary cutoff point of 5000 dithers was chosen). After 78,000 run-in revolutions, eight of the ten bearings reached the 50% level and required fewer dithers (640 to 1670 dithers). By 1.3 million revolutions all nine bearings tested (one bearing test was halted early) reached the 50% increase level requiring only between 137 and 730 dithers.

The benign-cage bearings (P/Ns 23–26) with sputter-coated races showed essentially the reverse behavior, in that dithering created sizeable torque bumps at 20K revolutions only. Figure 7 shows the maximum-to-minimum torque as a function of dithers at the various cumulative revolutions for P/N 25. Note that only at 20K revolutions is the torque increase swift and substantial. Table 4 gives a compilation of the results of the number of dithers required to increase the mean torque of the system prior to dithering (nominally ~0.007 N-m; 1.0 oz-in.) by 50% for the benign-cage bearings.

Wear Life

All the active-cage bearings continued to run without failure until the end of the test at 1.3 million revolutions. All the benign-cage bearings, P/Ns 23–26, failed at some point during the run-in period at 858K, 825K, 950K, and 1.4 million revolutions, respectively.

PHYSICAL FEATURES OF THE DITHER ZONE

The physical features of the dither zone were determined by scanning electron microscopy (SEM), stylus surface profilometry, and dimensional analysis of the torque-bump dither data.

The bearings were disassembled and the races examined after the last dither tests were completed at 1.3 million cumulative revolutions. A detailed examination of all of the bearing components is beyond the scope of this particular paper; however, features that appear to directly impact the formation of torque bumps will be presented.

Physical Features by SEM

SEM photomicrographs of the transfer films from the active-cage bearings generally show an apparently thin film on the wear track with a band of debris along both sides (Figures 8 and 9: Debris Bands). The width of the thin film was typically 0.76 to 0.87 mm. The transfer films (thin film plus debris bands) were on the order of 1.55 to 1.85 mm wide. Fourteen rectangular dither patches, equally spaced circumferentially, and corresponding to the dither zones produced by the 14 balls of the bearing, were observed on the inner and outer races (Figures 8 and 9: A dither patch in boxed area). A major portion of the dither patch overlays the thin film, although a small segment lies in one debris band. The dimensions of the dither patches (1.63 ± 0.10 mm $\times$ 0.90 ± 0.10 mm) are quite consistent from one bearing to the next, although the physical appearance can vary somewhat. Both dither patches contain a centrally located band where material appears to have been removed (Fig. 8: Area C and Fig. 9: Area A) when compared to similar areas outside the dither area. Differences between various bearing dither patches included such features as (a) gaps in material existing at both ends of the upper debris band (Fig. 8a: Areas A and B; Fig. 8b), and (b) two thin mounds of material near the edge of the dither patch that extend across the ball track (Fig. 9: Areas B and C). Note the appearance of a scuffed area to the left of the gap in Fig. 8b.

Physical Features by Profilometry

A surface profilometer was used on a very limited number of inner races in order to gain some insight into the surface texture of the patches. After the estimated surface curvature is subtracted, the profilometer data are presented in a linear format. Two cross-sectional areas on the inner race were traversed (Fig. 10a). The first was a land-to-land (cross-curvature) scan across the transfer film, purposely avoiding the dither patch, which would yield the thicknesses of the debris bands and possibly the thin film. The second scan was run across the dither patch but circumferentially. Fig. 10b. is an example of a land-to-land scan from P/N 19. The most prominent features are the two debris bands. The largest debris band has a maximum height of approximately 2.7 μm and a maximum width of ~600 μm, while the smaller debris band is ~1.5 μm high and ~250 μm wide. The total width of this particular portion of the transfer film is 1.85 mm, and the uniform thin-film portion is 1.0 mm wide. The thickness of the thin film is difficult to determine, but an estimate based on an extrapolation of the bearing surface profile on each side of the film and debris zones appears to be <0.2 μm. P/N 17 land-to-land results were similar to P/N 19 except that the debris bands were not as prominent.

The circumferential scan (Fig. 10c) showed a depression only when the stylus ran along the debris band from P/N 19. The following three features are observed: (1) a trough at both ends of the dither patch developed where significant amounts of material were excavated (Fig. 10c: Areas A and B); (2) much less material removed between the two troughs; and (3) a buildup of material beyond the dither zone (Fig. 10c: Areas C and D). The distance between the minima of the troughs for this particular patch is 1.74 mm and the circumferential length affected by the dithering is 2.01 mm. The troughs were measured to a maximum depth of ~2.3 μm (Fig. 10c:

Area B) and ~1.8 μm (Fig. 10c: Area A) below the surface of the debris band, which, as noted above, reached a maximum thickness of ~2.7 μm. Material was accumulated beyond the ends of ball travel and in line with the track. This collection of material reached a height above the surface of the debris band of 1.8 μm and 0.5 μm (Fig. 10c: Areas C and D, respectively). The P/N-17 circumferential scan again showed the same general characteristics, except that significantly more material was removed between the two troughs and no accumulation was detected outside the dither zone.

Physical Features by Torque Data

Due to the highly accurate positioning capability of the BTF motor, dimensional information in the circumferential direction can be calculated by converting the known number of motor steps into distance on the inner race, Eq. (2).

$$\chi = \frac{ZP\pi}{12800}\left\{1-\frac{1}{2}\left[1-\left(\frac{d}{P}\right)\cos\alpha\right]\right\} \tag{2}$$

χ = length of zone on race (mm)
Z = length of zone (motor steps)
d = ball diameter (mm)
P = pitch diameter (mm)
α = contact angle

For example, the 300 step dither should result in a 1.84-mm-long dither patch on the inner race. It is apparent from torque data, SEM photomicrographs, and surface profilometry that distinct surface features are present in or near the dither zone that result in a specific torque response. It was observed that the torque remained relatively unaffected in the interior portion of the dither area (i.e., between the two torque bumps), in particular at <5000 dithers (see Fig. 4). The average end-to-end length for this unaffected interior region on the inner races was 1.32 ± 0.16 mm (1σ). Beyond this length, extending to areas even outside the dither zone where the balls had not been, significant torque fluctuations were still observed. Calculations made on all the active-cage inner races show that the average length of the affected region is 2.49 ± 0.15 mm (1σ).

If the composition and frictional characteristics of the materials in the contact zones are assumed to remain constant during the various dithers, then significant changes in the transducer torque output can be considered to be the result of changes in the surface texture. This assumption is probably true for dithers between 0 and 5000, because the transfer film appears to be continuous and uniform between the two torque bumps. Integration of the torque signal should therefore provide an approximation of the surface texture.

Two examples of the integrated torque data along with the original raw torque data are shown in Fig. 11 for P/Ns 17 and 19 after 600 dithers. Integration results for both bearings suggest that not only are troughs formed at both ends of the dither patch but that the areas between the two

troughs also have been worn down slightly. The P/N 17 integration agrees with the profilometry results reported above, but P/N 19 results differ: the torque integration indicates a depression while the profilometry does not. The difference could be attributed to the fact that in surface profilometry the 2.5-μm-radius stylus traverses across only a small cross section of a single dither patch, whereas the torque data are the result of 14 dither patches being traversed simultaneously as the balls travel from one end of the dither patch to the other end.

DISCUSSION

The term torque bump, although appropriate with regard to sensor response, is actually a misnomer. Results have shown that the torque bump is primarily an excavated area (i.e., trough) where material has been transferred to adjoining regions. Bearings operating in an oscillatory motion without ball overlap can form significant torque bumps (one at each end of the dither zone) if enough material has been deposited on the races either by transfer from the cage or by some other deposition process.

If active-cage bearings are used, torque-bump development usually follows a well defined course. In the early stages of run-in (i.e., usually ≤20K run-in revolutions) torque-bump formation is absent or insignificant due to insufficient lubricant transfer from the cage to the races. Increasing the unidirectional run-in (>20K run-in revolutions) eventually leads to the transfer of enough material from the cage to the races to make possible the formation of torque bumps. Moreover, for all active-cage materials tested, the rate of torque-bump development *and* the maximum torque levels achieved monotonically increase with the number of run-in revolutions. These results suggest that a run-in of 78K revolutions or slightly less should suffice in order to minimize the development of torque bumps and still develop an adequate transfer film for reliable lubrication.

Equation (1) appears to describe the torque-bump formation data quite well; however, attempting to equate the parameters of Eq. (1) (i.e., α, β, and λ) with actual physical processes is difficult at this point. A plausible interpretation (there are certainly others) is presented as follows: During unidirectional run-in a very thin transfer film develops along with a thick debris band on each side. The debris bands are presumably composed of loosely held material, while the thin transfer film is significantly denser because of continual compression from numerous ball crossings during run-in. The onset of dithering causes a transverse creep (i.e., the balls are climbing the raceway shoulder) to occur, which shifts the dither patch partially into one of the debris bands. This transverse creep can be attributed to (a) a transverse creep force which occurs when a ball rolls and spins within a conforming groove and (b) misalignment.[21,22] It will be assumed that the debris band is the dominant factor in the formation of the torque bump.

In the initial stages of dithering a trough develops in the debris band where the balls are either accelerating or decelerating. We propose that the *rate* of material removal or trough formation is related to the parameter "β" in Eq. 1. Material from the trough can be displaced to a number of locations by a variety of scenarios: (a) during deceleration the balls skid and move or push material from the trough to the areas beyond the dither zone, (b) during acceleration material from one end of the patch transfers to the ball and is redeposited back to the same end after the ball has reversed direction and is coming to a "skidding stop", and (c) during acceleration the material is collected and then partially redistributed along the interior portion of the dither zone in all directions. (See the thick band toward the top of the photo in Fig. 9.)

The exponential increase in the torque-bump formation continues until the bearings reach an asymptotic limit where the exponential term approaches zero and the first term equals the constant value "α", usually between 1500 to 3000 dithers. Two factors can be responsible for

halting the exponential growth: (1) there might not be any loose debris left in the trough to be removed, and (2) from the onset of the first dither the balls passing over the underlying material cause it to become progressively denser, thereby slowing down the excavation process. Table 5 shows the values of "α" for bearings run-in to different times. The trend is for "α" to increase with run-in time or amount of material in the debris band in contact with the ball. Therefore, it is proposed that "α" can be correlated with the amount of excavated material, which is dependent on the thickness of the debris band or on the number of run-in revolutions. It should be cautioned that "α" values should be compared only for the bearings containing the same cage material, since different debris materials possess a variety of physical properties, (e.g., hardness, compressive strength, compressive ratio, and thermal conductivity) that could affect the excavation of material from the trough or the compaction rate.

The linear portion of Eq. (1) (λD) can be caused by further excavation of the remaining denser debris in the trough. (Coincident with this wear in the trough is additional wear of the thin transfer film which makes an undetermined contribution to the torque; see Fig. 8: Area C.) Profilometry results show that the thickness of the thin film is most likely <0.2 μm. SEM photomicrographs show that some thinning occurred in the thin film at 15,000 dithers. This thin film on the wear track appears to tenaciously resist wear, much more so than the bulk of the debris-band material. Except for the SM-cage and possibly the V-cage bearings, the thin films were capable of withstanding a minimum of 15,000 dithers in one location without failure (i.e., the torque remained stable).

The formation of the torque bumps in benign-cage bearings was opposite to that of the active-cage bearings. These bearings formed significant torque bumps only at 20K run-in revolutions. This result can be explained by the fact that enough MoS_2 is present to form troughs only in the 20K test. The MoS_2 removal is rapid toward the beginning of run-in. Subsequently, a very thin layer of dense material provides lubrication, but without replenishment it will be eventually worn away and removed from the contact regions. As in the active-cage bearing, the benign-cage bearings did not appear to show any erratic torque behavior in the dither zone between the two torque bumps even at 15,000 dithers. To insure minimal torque-bump formation, benign-cage bearings should be run-in at least 78K revolutions. Consideration must be also focused on the limited life of these bearings when used during continuous rotation. An increase in wear life can probably be obtained if, in addition to the races, the balls were also coated with MoS_2.

Figure 12 is an idealized representation of the typical dither patch, including the transfer film dimensions derived from the different measuring techniques discussed earlier. It summarizes in schematic form the various conclusions reached in this study.

SUMMARY

Proper conditioning of solid lubricated angular contact bearings must be performed whenever non-ball overlap oscillatory motions are expected to occur. Proper conditioning can minimize or delay the formation of torque bumps, which once formed can cause the torque of the bearing and therefore the mechanism to increase substantially. Evidence presented shows that torque bumps are primarily caused by troughs (excavated material) formed at the end of ball travel during dithering. New cages are currently under investigation that will attempt to combine the long lifetime of the active cages (continual replenishment of lubricant) with the ability to resist torque-bump formation. Bumps can be obliterated by causing the balls to run over them for extended times. A description of the "healing" process will be included in a future publication.

REFERENCES

1. H. E. Sliney, "Solid Lubricants," in *ASM Handbook*, Vol. 18, ASM International (1992) pp. 113-122.

2. M. R. Hilton and P. D. Fleischauer, "Lubricants for High-Vacuum Applications," in *ASM Handbook*, Vol. 18, ASM International (1992) pp. 150-161.

3. P. D. Fleischauer and M. R. Hilton, "Assessment of the Tribological Requirements of Advanced Spacecraft Mechanisms," in *Applications of Space Tribology in the U.S.A.*, L. E. Pope, L. L. Fehrenbacher, and W. O. Winer, eds., MRS, Pittsburgh, PA, Vol. 140, (1989) pp. 9-20.

4. P. D. Fleischauer and M. R. Hilton, "International Applications of Space Tribology," *Trib. Int.*, **23**, 2, pp. 135-139, (1990).

5. R. A. Rowntree and M. J. Todd, "A Review of European Trends in Space Tribology and Its Application to Spacecraft Mechanism Design," in *New Materials Approaches to Tribology: Theory and Applications*, L. E. Pope, L. L. Fehrenbacher, and W. O. Winer, eds., MRS, Pittsburgh, PA, Vol. 140, (1989) pp. 21-34.

6. E. W. Roberts, "The Lubricating Properties of Magnetron Sputtered MoS_2," *European Space Agency*, England, ESA-CR(P)-2624, (1987).

7. H. Kondo, K. Maeda, and N. Tsushima, "Performance of Bearings with Solid Lubricants in High Vacuum and High Speed Conditions," *Proc. JSLE. Int. Trib. Conf.*, Tokyo, Japan, pp. 787-792 (1985).

8. R. I. Christy, "Ion-Plated and Sputtered Coatings for Spacecraft Mechanisms," *Thin Solid Films*, **80**, pp. 289-296, (1981).

9. C. E. Vest, "Evaluation of Several Additional Dry Lubricants for Spacecraft Applications," *Lubr. Eng.*, **30**, 5, pp. 246-251, (1974).

10. M. J. Todd, "Solid Lubrication of Ball Bearings for Spacecraft Mechanisms," *Trib. Int.*, **15**, 6, pp. 331-337, (1982).

11. T. Kawamura, T. Honda, and N. Kawashima, "Study of Ball Bearings for Space Use," *Proc. Fourth Sym. on Space Mech. and Trib.*, Cannes, France, ESA Sp-299, pp. 101-107, (1990).

12. C. R. Meeks and J. Bohner, "Predicting Life of Solid-Lubricated Ball Bearings," *ASLE Trans.*, **29**, 2, pp. 203-213, (1985).

13. M. N. Gardos, "Theory and Practice of Self-Lubricated, Oscillatory Bearings for High-Vacuum Applications: Part I-Selection of the Self-Lubricative Composite Retainer Material," *Lubr. Eng.*, **37**, 11, pp. 641-667, (1981).

14. J. J. Bohner and M. N. Gardos, "The Effect of Composition on the Load-Speed Time-Dependent Oscillatory Wear of Selected Polymeric Self-Lubricating Composites," *Lubr. Eng.*, **43**, 5, pp. 347-350, (1987).

15. M. N. Gardos, "Self-Lubricating Composites for Extreme Environmental Applications," *Trib. Int.*, **15**, 5, pp. 273-283, (1982).

16. P. D. Fleischauer and R. Bauer, "Chemical and Structural Effects on the Lubrication Properties of Sputtered MoS_2 Films," *Trib. Trans.*, **31**, 2, pp. 239-250, (1988).

17. C. R. Meeks, "Theory and Application of Self-Lubricated Oscillatory Bearings for High-Vacuum Applications: Part II-Accelerated Life Tests and Analysis of Bearings," *Lubr. Eng.*, **37**, 11, pp. 657-667, (1981).

18. R. I. Christy, "Dry Lubrication for Rolling Element Spacecraft Parts," *Trib. Int.*, **15**, 5, pp. 265-271, (1982).

19. R. I. Christy and G. C. Barnett, "Sputtered MoS_2 Lubrication System for Spacecraft Gimbal Bearings," *Lubr. Eng.*, **34**, 8, pp. 437-443, (1978).

20. M. R. Hilton, R. Bauer, S. V. Didziulis, M. T. Dugger, J. M. Keem, and J. Scholhamer, "Structural and Tribological Studies of MoS_2 Solid Lubricant Films Having Tailored Metal-Multilayer Nanostructures," *Surface and Coatings Tech.*, **53**, pp. 13-23, (1992).

21. M. J. Todd, "Modelling of a Ball Bearing in Spacecraft," *Tribology International*, **23**, 2, pp. 123-128, (1990).

22. E. V. Zaretsky, "Liquid Lubrication in Space," *Tribology International*, **23**, 2, pp. 75-92, (1990).

Table 1. S106 Angular-Contact Bearing Description

Bore	30 mm
O.D.	55 mm
Material	440C Stainless Steel
Tolerance	ABEC-7
Balls	14 each, 7.14 mm diameter
Contact Angle	15°
Supplied Cage	Phenolic
Supplied Oil	None

Table 2. Cage Material Description

Symbol	Material Description	Type[1]	Hardness[2]
D	PTFE + microglass + MoS_2	active	70–72
R	PTFE + fiberglass + MoS_2	active	63–70
V	polyimide resin + 15% MoS_2	active	85–87
S	60% TFE + 40% bronze	active	63–64
SM	40% TFE + 55% bronze + MoS_2	active	68–70
Br	80 Cu + 10 Sn + 10 Pb	benign	—
Ph	Phenolic (As supplied)	benign	—

[1] The terms active and benign are used loosely to define the base or stock materials' lubricating ability. Depending on conditions, the Cu/Sn/Pb material can be considered active.

[2] Shore D hardness

Table 3. Bearing and Cage Combinations

P/N[1]	Cage	Cage Coating[2]	Race Coating[3]
11	D	NO	NO
12	R	NO	NO
13	SM	NO	NO
14	S	NO	NO
15	V	NO	NO
16	D	NO	NO
17	R	NO	NO
18	SM	NO	NO
19	S	NO	NO
20	V	NO	NO
23	Br	YES	YES
24	Br	NO	YES
25	Ph	NO	YES
26	Ph	YES	YES

[1] Part number

[2] rf-sputter deposited MoS_2 only

[3] MoS_2/Ni (*Ref. 20*)

Table 4. Dithers Required for 50% Increase in Torque Level

P/N	Revs	Dithers Needed for 50% τ Increase[1]
23	20K	1230
	78K	>5000 dither limit
	108K	>5000 dither limit
	308K	2250
24	20K	20
	78K	1480
	308K	>5000 dither limit
	525K	>5000 dither limit
25	20K	58
	78K	>5000 dither limit
	108K	>5000 dither limit
	308K	1350
26	20K	125
	78K	>5000 dither limit
	308K	>5000 dither limit
	1,300K	>5000 dither limit

[1] A limit of 5000 dithers was set. Beyond this point the significance of the data is limited.

Table 5. α Parameter from Equation 1

	Equation 1. 'α' at Cumulative Revolutions				
P/N	20K	78K	108K	308K	1300K
11-D	1.44	1.51	4.71	7.13	ND[1]
16-D	1.23	3.77	2.25	5.36	7.58
12-R	0.81	5.51	5.13	4.97	15.81
17-R	0.00	6.83	11.11	17.90	15.60
14-S	2.38	5.63	25.47	3.09	8.72
19-S	1.66	1.05	0.60	1.19	8.28
15-V	0.00	2.41	3.02	4.61	13.45
20-V	0.56	1.66	3.39	2.74	13.85
13-SM	5.81	3.66	15.66[2]	14.02	21.49
18-SM	0.00	1.36	3.97	12.61	7.87

[1] No data

[2] Taken at 200K revolutions

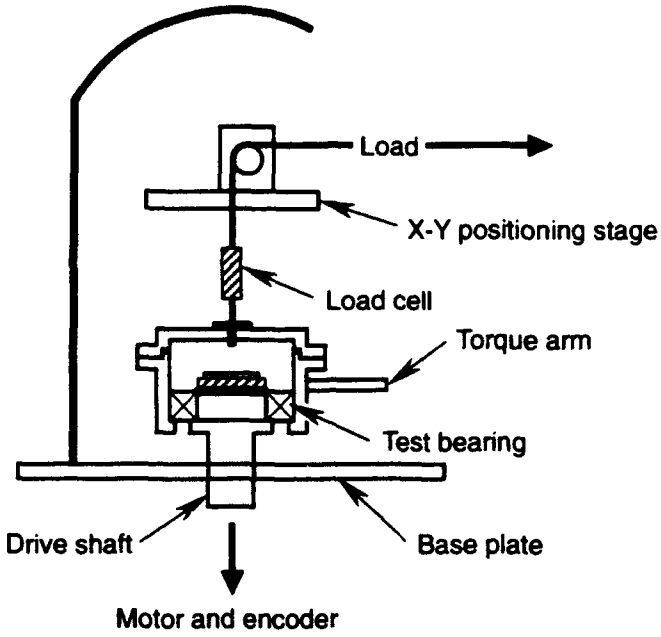

Figure 1. Bearing test fixture.

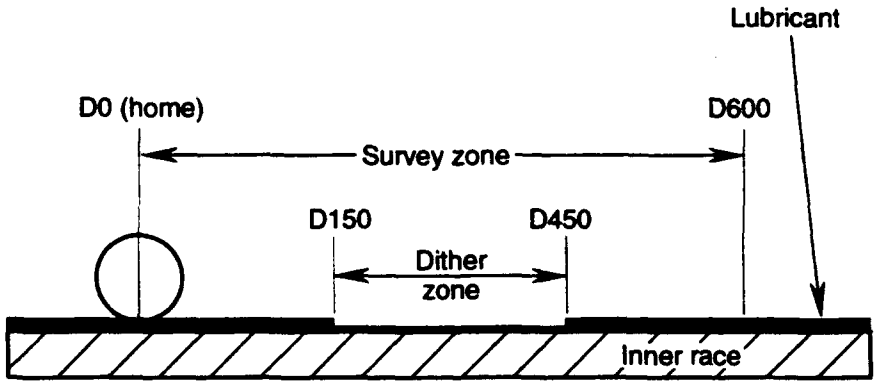

Figure 2. Bearing motion.

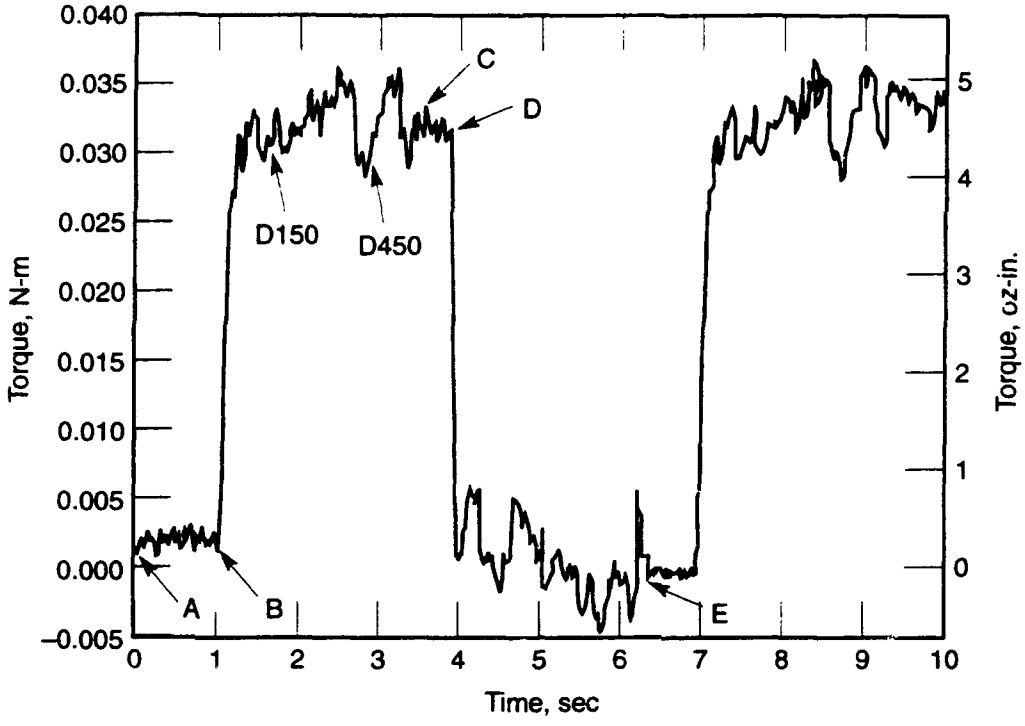

Figure 3. Survey torque scan: prior to dither.

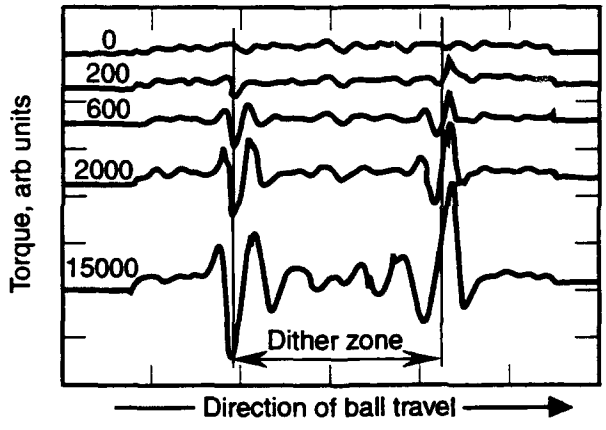

Figure 4. Torque bump increase as a function of dithers P/N 17; after 1.3 million revolutions.

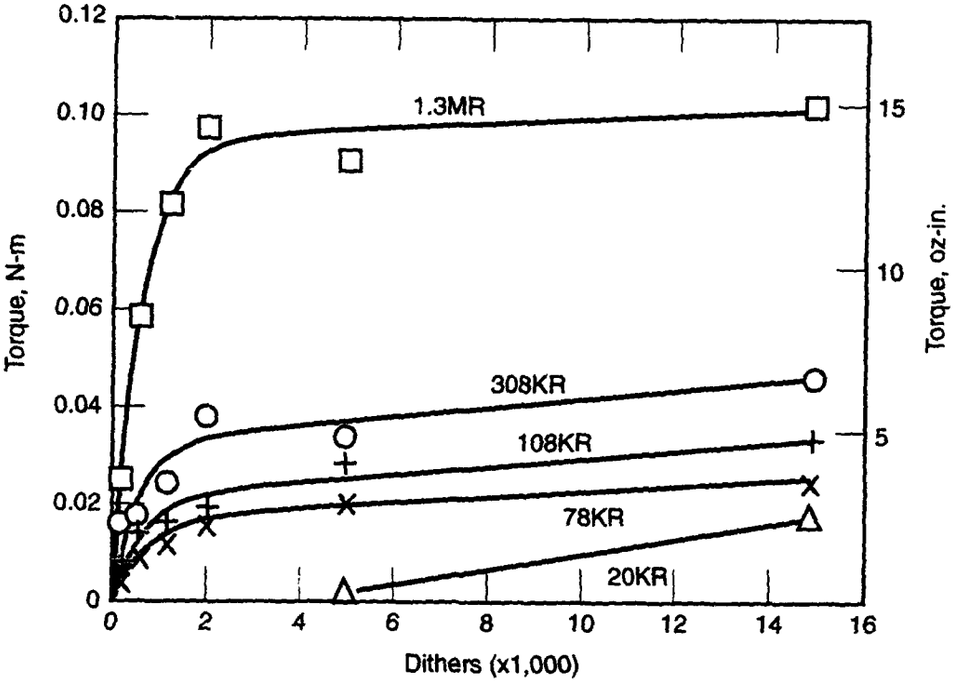

Figure 5. Torque vs dithers: active cage P/N 17.

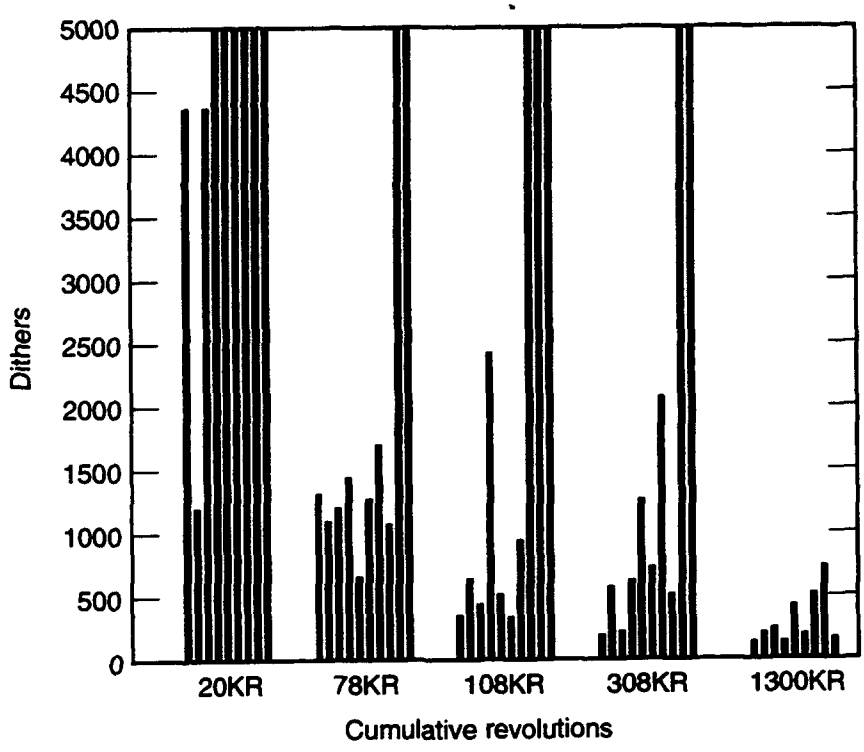

Figure 6. Torque increase vs revolutions: dithers required to increase torque by 50% (5000 dither limit—active cages only).

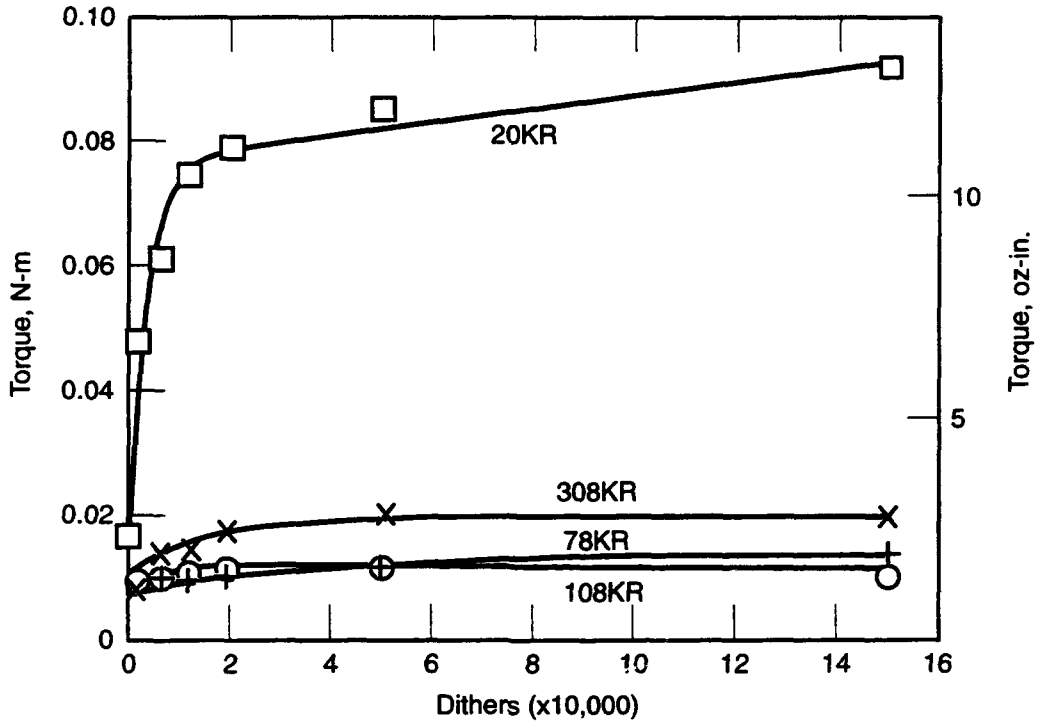

Figure 7. Torque vs dithers: benign cage P/N 25.

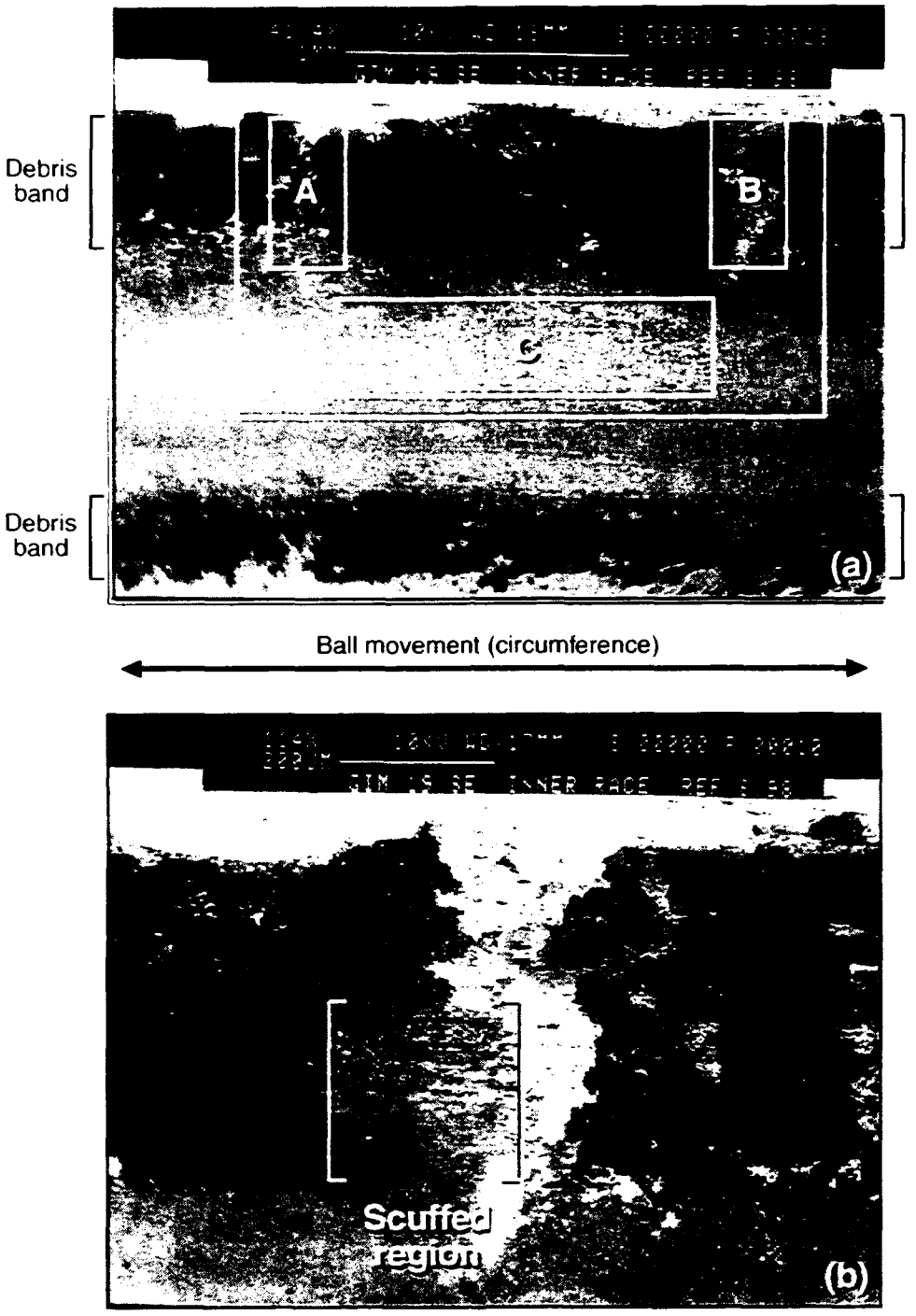

Figure 8. SEM photomicrographs of P/N 19 dither patch on inner race.
(a) dither patch
(b) enlargement of area B

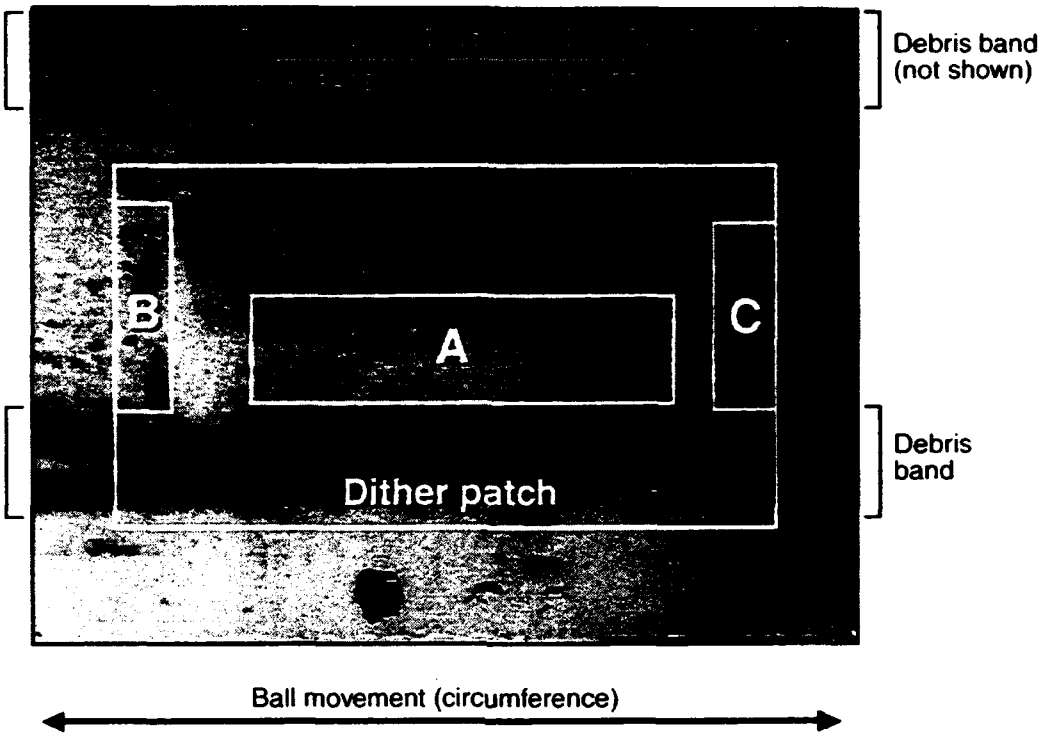

Figure 9. SEM photomicrograph of P/N 14 dither patch on inner race.

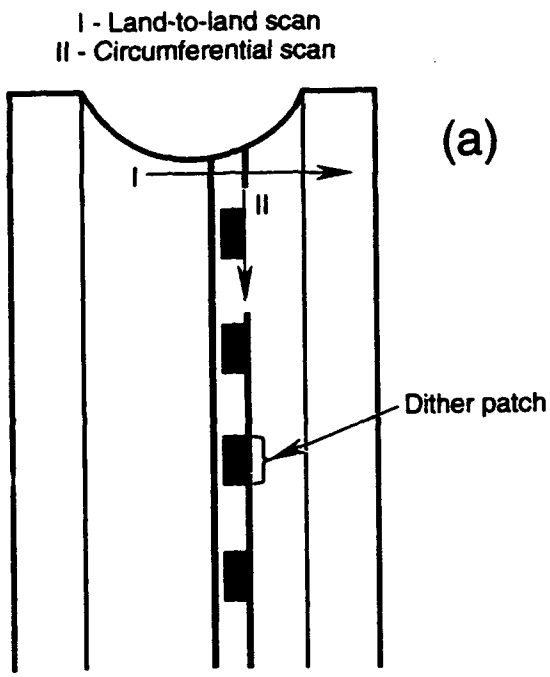

Figure 10. Surface profile of P/N 19 inner race.
(a) stylus paths

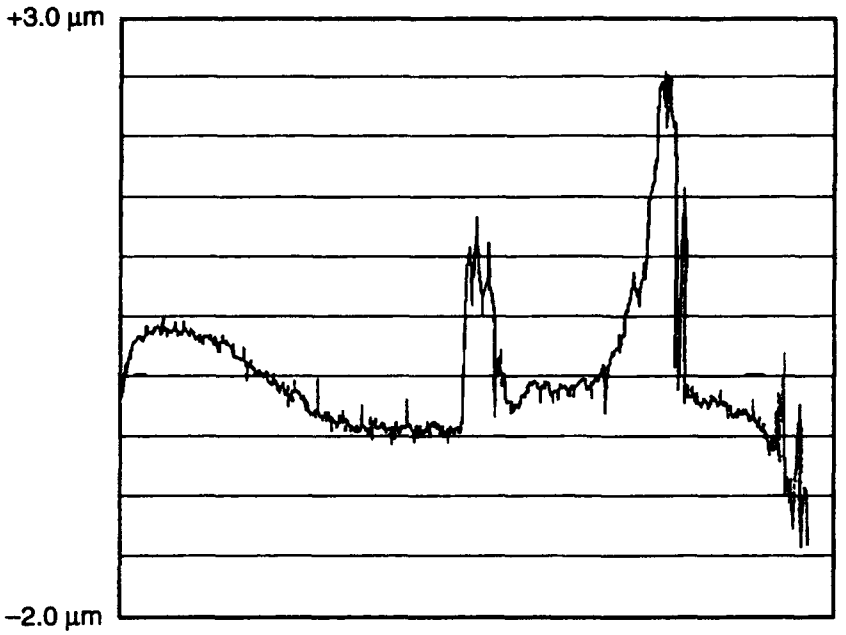

(b)

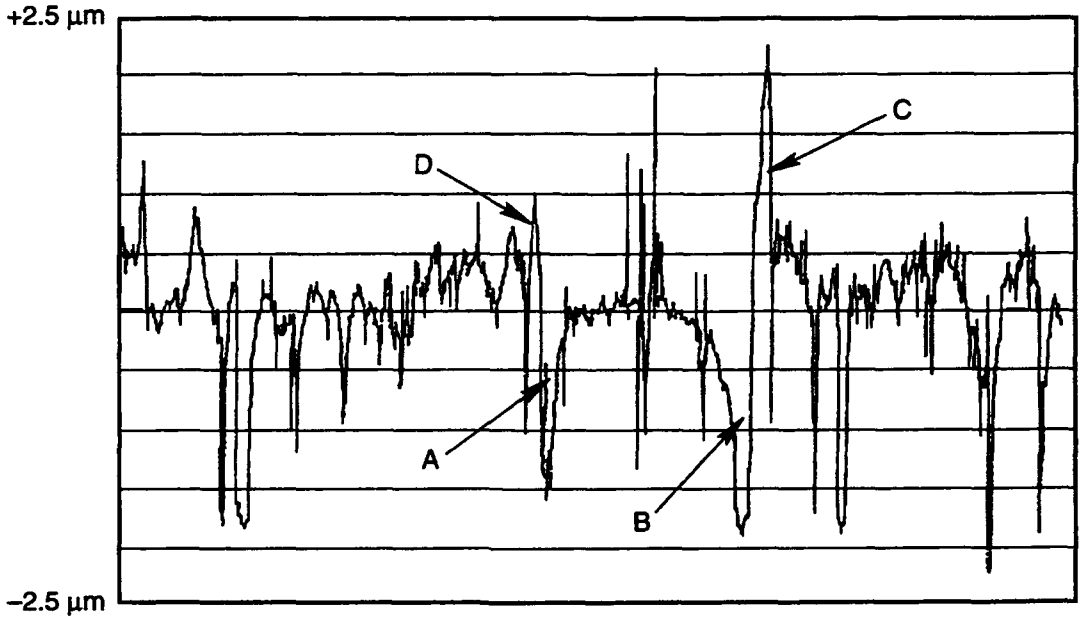

(c)

Figure 10. Surface profile of P/N 19 inner race (cont.).
(b) land-to-land (path I)
(c) circumferential (path II)

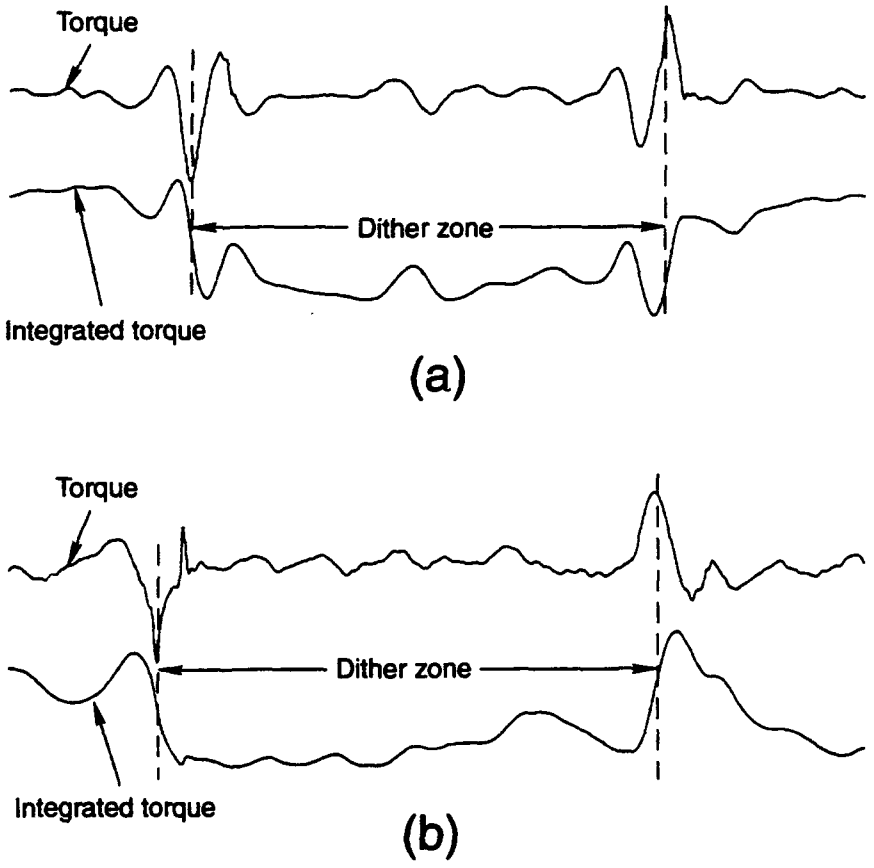

Figure 11. Partial of survey scan after 600 dithers.
(a) P/N 17
(b) P/N 19

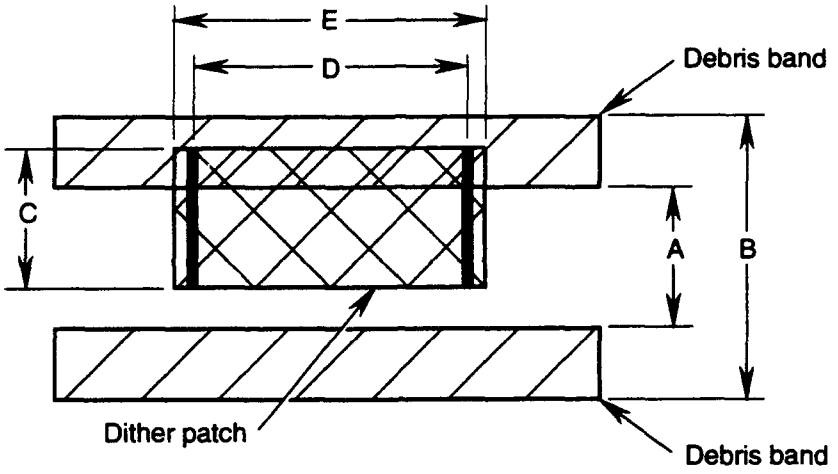

Location	Description	Dimension (mm)	Technique
A	Wear track width	0.8 1.0	SEM Profilometry
B	Transfer film width	1.6 to 1.9 1.9	SEM Profilometry
C	Wear patch width	0.9	SEM
D	Ball travel (inner race)	1.8 1.7 1.6	Theoretical Profilometry SEM
E	Torque affected length	2.5 2.0	Torque data Profilometry

Figure 12. Summary of dimensions.

TECHNOLOGY OPERATIONS

The Aerospace Corporation functions as an "architect-engineer" for national security programs, specializing in advanced military space systems. The Corporation's Technology Operations supports the effective and timely development and operation of national security systems through scientific research and the application of advanced technology. Vital to the success of the Corporation is the technical staff's wide-ranging expertise and its ability to stay abreast of new technological developments and program support issues associated with rapidly evolving space systems. Contributing capabilities are provided by these individual Technology Centers:

Electronics Technology Center: Microelectronics, solid-state device physics, VLSI reliability, compound semiconductors, radiation hardening, data storage technologies, infrared detector devices and testing; electro-optics, quantum electronics, solid-state lasers, optical propagation and communications; cw and pulsed chemical laser development, optical resonators, beam control, atmospheric propagation, and laser effects and countermeasures; atomic frequency standards, applied laser spectroscopy, laser chemistry, laser optoelectronics, phase conjugation and coherent imaging, solar cell physics, battery electrochemistry, battery testing and evaluation.

Mechanics and Materials Technology Center: Evaluation and characterization of new materials: metals, alloys, ceramics, polymers and their composites, and new forms of carbon; development and analysis of thin films and deposition techniques; nondestructive evaluation, component failure analysis and reliability; fracture mechanics and stress corrosion; development and evaluation of hardened components; analysis and evaluation of materials at cryogenic and elevated temperatures; launch vehicle and reentry fluid mechanics, heat transfer and flight dynamics; chemical and electric propulsion; spacecraft structural mechanics, spacecraft survivability and vulnerability assessment; contamination, thermal and structural control; high temperature thermomechanics, gas kinetics and radiation; lubrication and surface phenomena.

Space and Environment Technology Center: Magnetospheric, auroral and cosmic ray physics, wave-particle interactions, magnetospheric plasma waves; atmospheric and ionospheric physics, density and composition of the upper atmosphere, remote sensing using atmospheric radiation; solar physics, infrared astronomy, infrared signature analysis; effects of solar activity, magnetic storms and nuclear explosions on the earth's atmosphere, ionosphere and magnetosphere; effects of electromagnetic and particulate radiations on space systems; space instrumentation; propellant chemistry, chemical dynamics, environmental chemistry, trace detection; atmospheric chemical reactions, atmospheric optics, light scattering, state-specific chemical reactions and radiative signatures of missile plumes, and sensor out-of-field-of-view rejection.